https://doi.org/10.5194/essd-2019-113
Preprint. Discussion started: 5 July 2019

Open Access Earth System Science Data Discussions

The INSIEME seismic network: a research infrastructure for studying induced seismicity in the High Agri Valley (southern Italy)

Tony Alfredo Stabile[1], Vincenzo Serlenga[1], Claudio Satriano[2], Marco Romanelli[3], Erwan Gueguen[1], Maria Rosaria Gallipoli[1], Ermann Ripepi[1], Jean-Marie Saurel[2], Serena Panebianco[1,4], Jessica Bellanova[1], Enrico Priolo[3]

[1]Istituto di Metodologie per l'Analisi Ambientale, Consiglio Nazionale delle Ricerche, Tito (PZ), 85050, Italy
[2]Institut de Physique du Globe de Paris, Paris, F-75005, France
[3]Centro di Ricerche Sismologiche, Istituto nazionale di oceanografia e di geofisica sperimentale, Sgonico (TS), 34010, Italy
[4]Università degli Studi della Basilicata, Dipartimento di Scienze, Potenza (PZ), 85100, Italy

Correspondence to: Tony Alfredo Stabile (tony.stabile@imaa.cnr.it)

Abstract. The High Agri Valley is a tectonically active area in southern Italy characterized by high seismic hazard related to fault systems capable of generating up to M=7 earthquakes (i.e., the 1857 Mw 7 Basilicata earthquake). In addition to the natural seismicity, two different clusters of induced microseismicity were recognized to be caused by industrial operations carried out in the area: (1) the water loading and unloading operations in the Pertusillo artificial reservoir; (2) the wastewater disposal at the Costa Molina 2 injection well. The twofold nature of the recorded seismicity in the High Agri Valley makes it an ideal study area to deepen the understanding of nucleation processes of both natural and anthropogenic earthquakes and to improve the current methodologies for the discrimination between natural and induced seismic events by collecting high-quality seismic data. Here we present the dataset gathered by the INSIEME seismic network that was installed in the High Agri Valley within the SIR-MIUR research project INSIEME (INduced Seismicity in Italy: Estimation, Monitoring, and sEismic risk mitigation). The seismic network was planned with the aim to study the two induced seismicity clusters and to collect a full-range of open-access data to be shared with the whole scientific community. The seismic network is composed by 8 stations deployed in an area of 17 km x 11 km around the two clusters of induced microearthquakes and it is equipped with triaxial weak-motion broadband sensors placed at different depths down to 50 m. It allows to detect induced microearthquakes, local/regional earthquakes, and teleseisms from continuous data streams transmitted in real-time to the CNR-IMAA Data Centre. The network has been registered at the International Federation of Digital Seismograph Networks (FDSN) with code 3F. Data collected until the end of the INSIEME project (2019-03-23) are already released with open-access policy through the FDSN webservices and are available from http://www.fdsn.org/networks/detail/3F_2016 (https://doi.org/10.7914/SN/3F_2016; Stabile et al., 2016).

https://doi.org/10.5194/essd-2019-113
Preprint. Discussion started: 5 July 2019

1 Introduction

Anthropogenic seismicity has been documented since the 1920s when the subsidence due to the exploitation of the Goose Creek oil field (USA) was responsible of felt earthquakes (Pratt and Johnson, 1926). Even if McGarr (2002) proposed the use of different adjectives to describe earthquakes in which human activities have played some role, nowadays it is commonly accepted that the term induced seismicity is synonymous with anthropogenic seismicity; therefore, in this paper the two terms are considered as interchangeable.

The rapid increase of world population during the last 20 years as well as the economy development have raised the energy supply demand worldwide and, therefore, a variety of conventional and unconventional energy technologies are being developed to meet these needs, including shale gas production and geothermal energy (National Research Council, 2013, and references therein). Such energy technologies can be responsible of induced seismicity whose rate is particularly increased since 2008 (Ellsworth, 2013; Keranen and Weingarten, 2018). Unfortunately, different felt and moderate-to-large induced earthquakes reported in the literature (for a complete review see: Grigoli et al., 2017; Foulger et al., 2018; Keranen and Weingarten, 2018; Lee et al., 2019) caused damages to residential, industrial, and public buildings and/or fatalities thus increasing the public concern about the development of these energy technologies (National Research Council, 2013; Grigoli et al., 2017; Keranen and Weingarten, 2018).

Considering the strong socioeconomic impact of induced seismicity, the current research in this field has twofold importance: a) from a social and economic point of view it is useful for addressing the range of issues related to the induced seismicity, including the development of specific "best practice" protocols, monitoring strategies and traffic light systems, the correct definition of the associated hazard and risk, and the discrimination between natural and induced seismicity; b) from a pure scientific point of view the research it is fundamental for better understanding the processes involved in earthquake generation, the interactions among rock, faults, and fluids as a complex system, and how perturbations of the stress field, even of small size, may affect the stability of faults over time. On the other hand, the research activity in this field is often hampered by the lack of adequate monitoring networks or, more generally, by the lack of information (including field data and production data) which usually belong to private companies and the access is frequently restricted even when public research institutes are involved (National Research Council, 2013; Grigoli et al., 2017).

With the aim to overcome the issues related to data restrictions, different international scientific bodies, governments and geo-political entities are promoting open data policies in their research infrastructures and organisations. As an example, the International Seismological Centre (ISC, http://www.isc.ac.uk, last access: June 2019) currently collects data from approximately 150 agencies around the world providing an openly available bulletin that contains over 7.6 million seismic events, including induced events (Lentas et al., 2019). Another important permanent and reliable open access digital space for the induced seismicity community in Europe is the IS-EPOS Platform (https://tcs.ah-epos.eu, last access: June 2019), which belongs to one of the Thematic Core Services of the long-term plan EPOS (European Plate Observing System, https://www.epos-ip.org, last access: June 2019).

https://doi.org/10.5194/essd-2019-113
Preprint. Discussion started: 5 July 2019

The same open data policy has been adopted by the research project INSIEME (INduced Seismicity in Italy: Estimation, Monitoring, and sEismic risk mitigation), which was approved in 2015 by the SIR (Scientific Independence of young Researchers) program of the Italian Ministry of Education, Universities and Research (MIUR) and ended on 2019-03-23. Two Italian test sites have been selected for the project's research activities: (a) the Collalto area in the municipality of Susegana (Veneto Region, northeastern Italy), site exploited by Edison Stoccaggio S.p.A. for the storage of the natural gas; (b) the High Agri Valley (Basilicata Region, southern Italy) hosting the biggest on shore oil field in west Europe, managed by Eni S.p.A., and the Pertusillo water reservoir. The Collalto site is already being monitored since 2012 by a dense network of 10 seismic stations and one permanent GNSS geodetic station (https://doi.org/10.7914/SN/EV), which was the first Italian network providing data with open-access policy (Priolo et al., 2015).

In this paper, we present the INSIEME seismic network designed and developed in the framework of the INSIEME project for studying the induced seismicity in the High Agri Valley site. The broadband seismic network has been registered at the International Federation of Digital Seismograph Networks (FDSN, http://www.fdsn.org, last access: June 2019) with code 3F and the acquired data are released through open access. Section 2 details the seismic network from its layout to the acquisition, transmission and preliminary processing of data. Section 3 is instead focussed on the description of acquired seismic signals from the data quality of continuous data streams to the waveforms of recorded seismic events. Section 4 provides information on data availability. Finally, our discussions and conclusions are reported in Section 5.

2 The INSIEME seismic network

The High Agri Valley (hereinafter HAV) is a NW-SE trending intermontane basin formed during the Quaternary age along the axial zone of the southern Apennines thrust belt chain in southern Italy (Patacca and Scandone, 1989). It is one of the areas of Italy with the highest seismogenic potential with an expected maximum acceleration for an exceedance probability of 10% in 50 years within 0.25 and 0.275 g according to the national reference seismic hazard model (Gruppo di Lavoro MPS, 2004). Indeed the Italian historical seismicity catalogue CPTI11 (Rovida et al., 2011) reports seven earthquakes with Mw ≥ 4.5 in the HAV, including the 1857 Mw 7.0 Basilicata earthquake (Mallet, 1862; Burrato and Valensise, 2008) which was one of the most destructive historical earthquakes in Italy with 11,000 casualties and extensive damage throughout Basilicata, Campania, Apulia, and Calabria Regions. In addition to its natural seismicity, the HAV hosts energy technologies that cause two clusters of anthropogenic seismicity. More specifically, one of the two clusters (cluster A in Fig. 1) is continued-reservoir induced seismicity (Ml ≤ 2.7) linked to the seasonal water level fluctuation of the artificial Pertusillo Lake (Valoroso et al., 2009; Stabile et al., 2014a, 2015; Telesca et al., 2015; Vlĉek et al., 2018); the other cluster (cluster B in Fig.1) is fluid-injection induced seismicity (Ml ≤ 2) due to the disposal of the wastewater produced during the exploitation of the biggest onshore oil and gas field in west Europe at the Costa Molina 2 (CM2) injection well (Stabile et al., 2014b; Improta et al., 2015, 2017; Wcisło et al., 2018).

In this framework, the INSIEME seismic network has been specifically designed to achieve two main purposes: a) to study the seismic processes related to the occurrence of events belonging to the two clusters of anthropogenic seismicity; b) to provide the scientific community with new open-access high-quality seismic data for studying such phenomenon and for developing methodologies useful to discriminate between natural and anthropogenic events. The following points provide details of the network from its layout to the data acquisition and processing.

2.1 Seismic network layout

The INSIEME network is composed by 8 stations covering an area of about 17 km x 11 km, four of them around each of the two clusters of human-induced events (red circles in Figure 1). All the stations are equipped with broadband sensors installed in non-toxic PVC casings at different depths down to 50 m. Network layout definition was driven by several constraints, hereafter summarized:

- seismic stations must be deployed around the two clusters of induced events with a regular azimuthal coverage and distribution as regular as possible;
- the epicentral distance of the closest station must be less than the focal depth of events belonging to such seismicity clusters (Havskov et al., 2012);
- the average distance between stations should not exceed twice the event depth (Havskov et al., 2012) in order to have a good control on its estimate, taking into account that the studied clusters are characterized by shallow events of about 4-5 km focal depth (Serlenga and Stabile, 2019);
- as the studied clusters are characterized by shallow events, of about 4-5 km focal depth (Serlenga and Stabile, 2019), the average distance between stations should not exceed twice that depth (Havskov et al., 2012) to correctly estimate the event depth;
- high quality sites, possibly on hard bedrock and therefore without local ground effects, should be selected;
- recommended station locations must be as far as possible from strong noise sources such as main roads, town centers, industrial and quarry activities which are largely diffused in the HAV;
- station sites must be accessible for drilling operations;
- in areas belonging to the National Park "Val d'Agri - Lagonegrese", which covers large portions of the HAV territory (see file "INSIEME-network.kmz" provided in the Supplement), it is not possible to drill boreholes;
- stations sites should be covered by 3G communication link;
- seismic stations should guarantee continuous data acquisition in all weather conditions, even in the Winter season where the snow coverage could reach up to 1.5-2.0 m thickness for a couple of weeks;
- with the aim to provide an effective added value to the seismic monitoring of the HAV, station locations should not overlap existing stations of operating public and private seismic networks.

We performed seismic ambient noise measurements and geological surveys in order to find the most suitable sites according to these constraints, and we verified the access to the site (also for drilling operations of the shallow boreholes), data transmission conditions and unexpected potential sources of local noise. Afterwards, we evaluated the network performances following the approach proposed by Stabile et al. (2013) by considering different configurations of the potential sites that have met as more constraints as possible. The final network configuration is reported in Figure 1. It is worth noting that the minimum distances between stations (blue triangles in Figure 1) ranges between 2.7 km (INS6 and INS7 stations) and 5.4 km (INS1 and INS4), the distance of the closest station to each cluster is less than 4-5 km (the focal depth of induced events) and the INSIEME stations do not overlap stations belonging to other public (cyan triangles in Figure 1) and private (yellow triangles in Figure 1) seismic networks. Only INS8 station falls in the National Park "Val d'Agri - Lagonegrese" area and, therefore, the sensor of this station was installed on the surface.

2.2 Seismic stations

Considering that the main target of the INSIEME network consists in detecting and locating the anthropogenic microseismicity in the HAV (Ml ≤ 2.7), we equipped the seismic stations with triaxial weak-motion broadband sensors: six 0.05-100 Hz and two 0.0083-100 Hz Trillium Compact Posthole (TCPH) seismometers models, manufactured by Nanometrics Inc. (see Table 1). They provide a flat response to ground velocity up to 100 Hz. All data-loggers are manufactured by Nanometrics company, the 24-bit Centaur Digital Recorder with a dynamic range of 140 dB. Continuous acquisition of digital waveforms is provided by the INSIEME network at 250 Hz sampling rate. This choice allows data acquisition with a Nyquist frequency of 125 Hz, which is greater than the upper frequency bound of the broadband sensors (100 Hz), avoiding temporal aliasing effects on the acquired signals. The first installed station of the network was INSX (in operation between 2016-04-01 and 2017-01-24) whereas the other stations have been installed from 2016-09-23 (see Table 2).

With exception of the INS1 station which was initially connected to the electric power grid of the Montemurro Cemetery, power supply for all stations is provided by solar panels and batteries. Each station is equipped with a 270 W solar panel and two 12 V, 100 Ah batteries connected in series to output 24 V, which allows the instruments to work with less current. Solar panels are installed on 2 m high poles in order to prevent snow covering the Winter season (see Figure 2a), then the solar charge controller, the two batteries, the power supply circuit, the data-logger and the router are housed in a small cabin (Figure 2b). Corrugated cables allow the passage of sensor cables from the cabin to the borehole (Figure 2b). Each borehole is closed by a manhole (Figure 2b) and the PVC casing is coupled to the soil by cement grout filling the space between the hole and external surface of the PVC casing from the bottom to the surface (Figure 2c). The PVC casing is not in the manhole in order to leave room for installing sensors on the surface (Figure 2d). A 2 m high netting surrounding an area of about 2.5 m x 2.5 m, protects each station from wild or grazing animals.

The broadband seismometers installed in boreholes are equipped with a coupling system (Figure 2e) developed by the National Institute of Oceanography and Experimental Geophysics of Italy (OGS). The inclination of each borehole from the surface to the bottom has been measured with an in-place inclinometer (Jewell Instruments, Model 906 Little Dipper). We found that the 5 shallow boreholes of 6 m depth (stations INS2, INS3, INS4, INS5, and INS6) have inclination at the bottom less than one degree and one of the two 50 m deep boreholes deviates 1.6 degrees at the bottom (station INS1). On the other hand, the second

https://doi.org/10.5194/essd-2019-113
Preprint. Discussion started: 5 July 2019

50 m deep borehole (station INS7) is highly deviated over 20 m depth. Indeed, at 14 m depth we measured an inclination of 1.7 degrees, increasing up to 2 degrees between 16 m and 20 m and over 6 degrees beyond 24 m depth. Since the two deeper boreholes host the 0.0083-100 Hz TCPH seismometers model, which operates with a maximum tilt of 2 degrees, we installed the seismometer of station INS1 at 50 m depth whereas the INS7 one was installed at 14 m depth. Table 2 indicates the sensor depths of each borehole station.

Furthermore, seismometers at 6 m depth are installed by a modular developed by OGS in order to control the orientation of the horizontal components (Figure 2d). For the two seismometers placed at 14 m and 50 m depth, respectively, the orientation of their horizontal components was unknown because of the impossibility to use a longer non-rotating arm. In this case we estimated their azimuthal orientation with respect to a reference station by applying a methodology similar to that proposed by Zheng and McMechan (2006), based on the maximization of the cross-correlation among the horizontal traces of adjacent sensor pairs. Of course, for each pair of adjacent sensors we assume the condition of plane wave approximation which is satisfied if the distance d between sensors is much less than dominant wavelength λ of the recorded signal ($d \ll \lambda$). Therefore, the signals recorded by the two sensors must be filtered with a cut-off frequency $f_c \ll Vd^{-1}$, with V the lowest seismic velocity of the medium.

Afterwards, for each angle θ ranging from 0 to 360 degrees with a step size of 0.5 degrees, we computed the normalised cross-correlation between the North component of the signal recorded by the reference station (Sr_N) with the first horizontal component of the signal recorded by sensor with unknown orientation and rotated counter-clockwise by the angle θ (Su_1^θ). In addition we computed the normalised cross-correlation between the East component of the signal recorded by the reference station (Sr_E) with the second horizontal component of the signal recorded by sensor with unknown orientation and rotated counter-clockwise by the angle θ (Su_2^θ). For each angle θ, the maximum value of the cross-correlation between Sr_N and Su_1^θ (A^θ) and between Sr_E and Su_2^θ (B^θ) were retrieved. Then, the sensor orientation with respect to the reference sensor was given by the following Eq. (1):

$$\theta^{BEST} = \theta : \max_{0^\circ \le \theta \le 360^\circ} \left(A^\theta B^\theta \right), \quad (1)$$

where θ^{BEST} is the angle for which the product between A^θ and B^θ is maximum. By applying Eq. (1) over N recordings, we obtained N estimates of θ^{BEST}; therefore, we evaluated the weighted arithmetic mean and the weighted standard deviation of all the N estimates, with $W_i = (A^\theta B^\theta)_i$ the weight of the i-th θ_i^{BEST}.

For station INS1 we used as reference the station INSX, whose sensor was only 70 m distance from the borehole sensor of station INS1 and acquired simultaneously with station INS1 from 2016-10-12 to 2017-01-24 (Table 1 and Table 2). We applied a bandpass filter to the seismic recordings with corner frequencies of 0.1 Hz and 0.5 Hz because we surely satisfy the relation $f_c \ll Vd^{-1}$ and because in this frequency range we can use also the seismic ambient noise for determining the rotation angle; in this frequency range, indeed, noise contains the microseismic peak (Longuet-Higgins, 1950) between 4-8 s (0.125-0.250 Hz) which is very coherent. To compute the rotation angle we used recordings of 3 earthquakes (Mw 6.5 Central Italy earthquake of 2016-10-30, Mw 5.4 Greece earthquake of 2016-10-15, and Mw 7.9 Papua New Guinea earthquake of 2017-

https://doi.org/10.5194/essd-2019-113
Preprint. Discussion started: 5 July 2019

01-22) and seismic ambient noise data of different durations (20 minutes, 1 hour, and 2 hours). The final estimate of the rotation angle for the sensor of station INS1 is 307.8±0.4 degrees counter-clockwise to the North.

For station INS7 we used as reference the station INS1 after its alignment to the North because the two stations are both equipped with the same broadband sensors (Table 1). The two stations acquire data simultaneously since 2017-03-23, when the sensor of INS7 station was installed in the borehole (Table 2), and they recorded several teleseisms. We used the surface waves of 12 selected teleseism with Mw≥6.9 occurred between November 2017 and August 2018. The distance between stations is 11 km; therefore, we applied a low-pass filter to the seismic recordings with a corner frequency of 0.05 Hz which satisfy the relation $f_c \ll Vd^{-1}$ even if we consider a Rayleigh wave speed as low as 2.8 km s^{-1}. The final estimate of the rotation angle for the sensor of station INS7 is 43.8±0.3 degrees counter-clockwise to the North.

Dataless of all the INSIEME seismic stations, which include comprehensive information of each station and the respective instrument response, are provided in the Supplement.

2.3 Seismic data acquisition, data transmission, visualization and preliminary processing

Seismic data are transmitted in real time by 3G mobile system. The modem/router adopted is Teltonika RUT-500; this device is capable of communicating with every 3G Italian mobile network and has also an integrated 4-port RJ-45 10/100Mbps Ethernet switch for the Local Area Network. The mobile telecommunication provider allocates a dynamic public IP address to the WAN-interface of the router; for this reason, the system cannot be continuously reached from an external network, as the address may change. Hence it was necessary to configure a Dynamic DNS (Domain Name System). A dynamic DNS host name is linked up to the router's dynamic IP address. Whenever the IP changes, a dynamic DNS client (configured on the Teltonika RUT-500) will send an update to Dynamic DNS service with the current IP address and then the system propagates the DNS change to the Internet within few seconds. In this way the end user is able to reach directly each seismological station, both for management and data acquisitions. Nanometric Centaur digital recorder uses a data streaming protocol called SeedLink. This is a transmission protocol system used to make the data available on the Internet, because it supports the "Internet Protocol suite TCP/IP" (Transmission Control Protocol / Internet Protocol). The router Teltonika RUT-500 is compliant with SeedLink, and therefore adopted as transmit tool.

Since it is not uncommon for routers to encounter problems that prevent the internet connection, each station is equipped with a programmable time switch that periodically (in our case once a week) disconnects for few seconds the power supply of the router. When the router restarts, the Centaur data-logger is able to send missing data to the CNR-IMAA (National Research Council of Italy, Institute of Methodologies for Environmental Analyses) Data Centre. Despite these precautions, sometimes data gaps may occur due to prolonged temporary absence of the signal or other minor transmission problems. For this reason, a 16 GB SD memory card is mounted on each Centaur which allows the local storage of about 6 months of data. After a check on data gaps for each year and for all the components of each station, the missing data range between 0.0019% (channel CHE of INS8 station, year 2018) and 2.7564% (channel CHZ of INS6 station, year 2017) of the whole data. All the gaps due to transmission problems have been filled by using data saved on each SD memory card. The unfilled gaps are related to a programmed temporary shutdown of a station (e.g., maintenance, firmware update) or to undesired problems occurred to a specific station. As an example, the missing data of station INS6 of about 2.8% for the year 2017 (corresponding to a cumulative time of about 10 days out of 365 days) is due to a misconfiguration of the solar charge controller on which the night light function was erroneously activated (during sunshine the power was switched off). The problem was understood and definitively solved on 2017-01-24 at 09:52 UTC. After this configuration correction, the gaps at station INS6 have become comparable to those observed to the other stations of the INSIEME seismic network.

In the CNR-IMAA Data Centre there is a Linux server for data acquisition, storage and processing. The server has been equipped with a hardware RAID controller (redundant array of independent disks), configured as a "RAID 1" disk mirroring, to protect the data in case of drive failure. Our configuration features two 4 TB hard disks (i.e. 8 TB RAW space) in RAID 1 mode, ensuring a N+1 disk redundancy and a 4 TB total storage capacity. This configuration is an optimal choice for applications requiring high availability. In the future, we will upgrade the system by means of a Network Attached Storage (NAS) in order to store data as well as to enhance the system performance and availability. Furthermore, on this server the TCP/IP-based SeedLink standard compliant SeisComP3 (www.seiscomp3.org) software runs for seismological data acquisition. It acquires data in real-time from the INSIEME stations and neighbour stations, store them in a miniSEED file structure and it is able to make those data available through various standard protocols: seedlink for real-time flow, arclink and FDSN webservices for archived data requests. This SeisComP3 software also holds the stations metadata and an event database. A schematic view of the data flow from the data-logger to the Data Centre is displayed in Figure 3.

A dedicated intranet system, WebObs (Beauducel et al., 2010), is used to plot in near real-time numerical strip-chart (SefraN) of a representative subset of the configured stations. This SefraN is used to manually identify any event present in the data (Figure 4, top panels). It is associated to the Daybook, a database of all the events that have been identified in the data, whether they can be located or not. Some regional and global events are prefilled with information gathered from INGV and USGS FDSN event webservices (http://www.fdsn.org/webservices). When a new event is identified, the information is sent to the SeisComP3 database (Figure 4). The event is then manually picked and located (Figure 4, bottom panel) with SeisComP3 Origin Locator Viewer (scolv), using the 1-D velocity model from Improta et al (2017). The WebObs Daybook displays the event information gathered from the SeisComP3 FDSN webservice.

3 Acquired seismic signals

3.1 Data quality in terms of background noise level

One of the most important goal of a seismic network is to provide high quality records of a seismic event from a number of stations as large as possible and with a good azimuthal coverage; therefore, if the seismic noise is high at different sites the benefits of modern equipment with large dynamic range are compromised (Havskov et al., 2012).

It is well known that the background noise is due to several factors like temperature changes, weather conditions and anthropogenic noise. The first two factors generally produce low-frequency noise (<0.05 Hz) whereas the latter usually contains high frequencies (> 1 Hz). In addition there is also the microseismic noise in the range 4-8 s generated by the sea activity (Longuet-Higgins, 1950). Since most of the broadband sensors of the INSIEME seismic network have flat response in the range 0.05-100 Hz (see Table 1) and the seismic network is primarily designed to observe microearthquakes, the main goal of our sensor installations is to attenuate the anthropogenic noise. Several studies have already focused on the attenuation of such specific kind of noise (Young et al., 1994; Withers et al., 1996) or on the attenuation of the noise over a broader range of frequencies including both low and high frequency noise (Hutt et al., 2017). The results of such studies indicate that a successful reduction of the noise is achieved by placing seismic instruments at depth and in the rock instead of soil. Indeed, surface layers above the rock, which have low seismic wave velocities, tend to trap the anthropogenic noise and produce site amplification effects. Furthermore, installing seismic sensors at depth in PVC casing has been demonstrated to be an effective way to attenuate the diurnal temperature variation (Spriggs et al., 2014), as we did for our stations.

With the aim to evaluate the seismic noise attenuation at depth for our stations we first installed the sensors of each station on the surface for a period of about 6 months and subsequently we moved the sensor inside the PVC casing at depth (Table 2). The only one exception is the station INS1 whose sensor was directly installed at 50 m depth because at the same site there was in operation the surface station INSX until 2017-01-24 (Table 2). By selecting continuous data streams acquired by INS1 and INSX stations with duration of three days from 2017-01-05 to 2017-01-07, characterised by high natural and anthropogenic noise level, we computed the Probabilistic Power Spectral Densities (McNamara and Buland, 2004). Figure 5 show the comparison of the Probabilistic Power Spectral Densities (hereinafter PPSD) obtained for each component of INS1 and INSX stations in the period range 0.01-20 s (frequency range 0.05-100 Hz). The colour palette indicates the probability (in percentage) to have a certain noise level as a function of the period. The two grey lines in each panel indicate the High and Low Noise models, respectively, obtained by Peterson (1993) which are used as reference. The two horizontal components of INS1 station (CH1 and CH2) are compared with the two horizontal components of INSX station (CHE and CHN) and the vertical components (CHZ) of the two stations are compared each other. It is possible to observe that the noise level is more regular at 50 m depth than at surface and that for periods below 1 s (frequencies above 1 Hz) we have a reduction of the noise level of about 10 dB on average and up to 20 dB. In Figure 5 periods above 20 s (frequencies below 0.05 Hz) are highlighted in grey because in such period range it is not possible to compare the PPSD of the two stations since only the sensor of INS1 stations has flat response up to 120 s (see Table 1) and, therefore, only its PPSD is reliable.

We computed also the PPSD on continuous data streams acquired by INS1, INS2, and INS4 stations from 2017-12-26 to 2017-12-30, a period again characterised by high natural and anthropogenic noise level. It is possible to note (Table 2) that INS2 and INS4 stations are equipped with sensors installed at 6 m depth. Figure 6 shows the comparison among the PPSD obtained for the horizontal and vertical components of each station in the period range 0.01-20 s (the sensors of stations INS2 and INS4 are 20s-100Hz Trillium Compact Posthole). In this case we do not observe a significant difference of PPSD between a sensor installed at 50 m depth (as for INS1 station) and a sensor installed at 6 m depth (as for INS2 and INS4 stations), hence we can argue that installing a sensor at 6 m depth is enough to have a noise reduction in the period range 0.01-20 s similar as when installing a sensor at 50 m depth.

In order to better understand how the installation of sensors in PVC casing at least 6 m depth is an effective solution for the seismic noise attenuation, we compared spectrograms over long-time continuous data streams (41 days from 2017-03-02 to 2017-04-11) acquired by the two seismic stations INS5 and INS6 of the INSIEME network. As evinced in Table 2, the broadband sensor of INS5 station was installed at 6 m depth during the whole period of observation; on the other hand, the broadband sensor of INS6 station was first placed on surface until 2017-03-22 and then moved in the shallow borehole at 6 m depth. Figure 7 shows the comparison of spectrograms at the two stations over the whole investigated period. It is very clear the noise attenuation of about 20 dB at station INS5 with respect to station INS6 before 2017-03-22, particularly along the two horizontal components, but the noise levels are comparable in the period of time when both the stations have their respective sensors installed at depth. After 2017-03-22 it is possible to observe that the high frequency (> 1 Hz) day-night succession of INS5 station is little bit more pronounced than the day-night succession of INS6 station because the former is closer to the urban area of Sarconi town than the latter. Finally, it is interesting to observe as expected the increase of the microseismic noise in the range 4-8 s generated by the sea activity during storms (e.g., in the period 06-09 March 2017 as effects of a strong Mistral event in the Tyrrhenian Sea); this phenomenon is masked by the high noise level when the sensors are placed on surface.

3.2 Data quality in terms of local ground effects

Local seismic amplifications due to sensor installation on soft ground can greatly affect spectral analyses of low and moderate earthquakes, the broad-band recording can be useless and the short period signals may be unrepresentative (Havskov et al., 2012). The absence of meaningful site effects was beforehand assessed for properly choosing the future locations of each seismic station of the INSIEME network. In order to check the validity of our choice and the quality of seismic signals a further assessment of the negligible site effect on recorded data has been carried out.

To this purpose earthquake data have been selected from the preliminary catalogue of the SeisComp3 database (see section 2.3). With the aim to have more accurate locations, the events have been relocated by means of NonLinLoc code (Lomax et al., 2000) in a 3-D velocity model of the area (Serlenga and Stabile, 2019), allowing us to distinguish three different categories of seismic events:

a) injection-induced earthquakes (IIE hereinafter), whose epicenters belong to the cluster B located NE of the Pertusillo lake and close to the CM2 injection well (see Figure 1). We also increased the number of IIEs by using a template-matching algorithm, that we are still implementing, based on the array processing of nearby stations proposed by Gibbons and Ringdal (2006). In this way we were able to use 164 injection-induced earthquakes;

b) reservoir-induced earthquakes (RIE hereinafter), belonging to the cluster A located SW of the lake (see Figure 1), for a total number of 56 events;

c) local earthquakes (LE hereinafter) located in the HAV. In particular, only events with a magnitude greater than 1.5 were selected, for a total number of 33 events. In that way, we guaranteed that the highest number of stations had recorded the selected data.

https://doi.org/10.5194/essd-2019-113
Preprint. Discussion started: 5 July 2019

In addition to earthquake data, five hours of seismic noise data (SN hereinafter) were extracted in the time window 9:00 – 14:00 UTC of 2018-11-26.

In order to assess the presence of possible local ground effects at the sites where the stations were installed, the selected data were analyzed by applying the Horizontal to Vertical Spectral Ratio technique (Nakamura, 1989), both to earthquakes (HVSR) and noise data (HVNSR).

To this purpose, each component of earthquake data was cut in time windows which allowed to discard as much as possible the pre- and post-signal noise. For IIE, RIE and LE data we chose 8 s, 16 s and 32 s wide time windows, respectively, with a corresponding minimum frequency of 0.125 Hz, 0.0625 Hz and 0.03125 Hz. In order to have reliable estimates the spectra were evaluated starting from 10 times the respective minimum frequency (i.e., 1.25 Hz, 0.625 Hz and 0.3125 Hz). The difference in the selected time windows is related to the dissimilar durations of recorded signals of each category of earthquakes. Before computing the Fast Fourier Transform, the mean and the trend were removed from the time series and signals belonging to any data category were tapered by applying a Tukey window with 5% bandwidth. Then, the computed spectra were smoothed by means of Konno-Omachi function (Konno and Omachi, 1998), with a bandwidth coefficient equal to 40. The HVSR for each earthquake was retrieved from the arithmetic mean of the horizontal amplitude spectral components (EW and NS) over the vertical amplitude spectral component (Z) of the acquired signal, that is:

$$HVR = \frac{EW+NS}{2Z}. \quad (2)$$

Finally, the average HVSR for each station and earthquake category was computed, along with the ±1σ (one standard deviation). The choice of performing such an analysis on different types of earthquakes, characterized by an heterogeneous location in space, was related to look for possible source and directivity effects on the consequent HVSR measurements.

The 5 hr long SN data, on the other hand, were cut in 130 s wide non-overlapping time windows, which spanned the total temporal extension of the recording, providing a total number of 138 signals with a spectral resolution of 0.007 Hz. The retrieved time series were processed in an analogous way to the one described before for earthquake data by means of the Geopsy software (Geopsy project, http://www.geopsy.org, last access: June 2018). For each time window and station, the HVNSR was retrieved, taking into account that the horizontal spectrum was computed as the squared average of the two horizontal (EW and NS) components:

$$H = \sqrt{\frac{EW^2+NS^2}{2}}. \quad (3)$$

Finally, the average HVNSR of each station was computed, along with the ±1σ.

The retrieved HVSR and HVNSR are represented in Figure 8. We can assert that the most of the stations are characterized by an almost flat H/V curve, independently of the adopted dataset. Furthermore, we separately verified that the choice of an arithmetic mean or a squared average of the two horizontal components is almost completely irrelevant to the consequent HVSR or HVNSR measurements. The arithmetic average adopted for earthquake data analysis allowed to equally weight possible amplitude peaks related to directivity and azimuthal effects in the HVSR computation. On the other hand, the squared average, which generally overestimates the arithmetic average and which was adopted for analyzing the ambient noise data, did not produce higher amplitude peaks: indeed, the retrieved HVNSR curves are flatter than HVSR ones.

In Figure 8 we observe very low site amplifications, except for INS5 seismic station, where a small peak at about 3.5 Hz can be noticed and for INS6 whose HVSR function has a slight amplification between 0.8-3.0 Hz. Some detailed considerations must be done on the results related to station INS1. Previous analyses performed at the same site with ambient noise and earthquake data, by using both a seismometer and an accelerometer located at the surface, and with geological and geophysical (Electrical Resistivity Tomography) surveys allowed to approximately estimate the depth of the bedrock at about 50 m (Giocoli et al., 2015). Indeed, an amplitude peak between 2 and 3 Hz in the retrieved H/V curves was clearly observable. By looking at Figure 8, this peak is no more present, confirming that the installation of INS1 at 50 m depth allowed us to reach a more rigid (higher acoustic impedance) layer; in addition to it, during perforation operations, it was clearly observed at that depth a sharp lithological change between less and more competent rocks. The low amplitude peaks at about 4-5 Hz, 9 Hz and 11 Hz are another interesting element related to HVSR curves at INS1 seismic station. Furthermore, we observe that the highest frequencies peaks are not present in the HVNSR curve. We might interpret these differences as the effect of the down-going wavefield.

3.3 Induced microearthquakes, local earthquakes, and teleseisms

The continuous data acquisition by the INSIEME seismic network allowed to manually detect, by a visual inspection of recordings through SefraN tool, a total number of 856 local natural and induced earthquakes between September 2016 and December 2018. Then, these were preliminarily located in the 1-D velocity model by Improta et al. (2017) by adopting Hypo71 algorithm (Lee and Lahr, 1972) embedded in SeisComP3, allowing us to better distinguish the three different categories of seismic events already introduced in the previous section (3.2): IIE, RIE, LE. To this purpose, and particularly to better locate local event outside the INSIEME network, we build a virtual seismic network composed by 11 seismic stations of the Italian National Seismic Network (FDSN codes: IV and MN) managed by the Italian National Institute of Geophysics and Volcanology (INGV), 7 stations belonging to the Irpinia Seismic Network (Weber et al., 2007; Stabile et al., 2013; FDSN code: IX), and MARCO station belonging to the Geofon network (FDSN code: GE), the latter installed south of Tramutola town in the framework of a joint scientific cooperation between GFZ-Potsdam and CNR-IMAA institutes; all the stations of the virtual network are located within about 60 km distance from the centre of the INSIEME network.

Here we report the main inferred features for each earthquake category (IIE, RIE and LE), in terms of both seismic signal properties and hypocentral locations:

a) IIE: a total number of 42 injection-induced seismic events was manually detected. These were identified because of their first arrival at INS1 seismic station, which is the closest receiver to the seismicity cluster induced by fluid-injection operations at the CM2 well (cluster B in Figure 1); furthermore, their signals are characterized by a difference between the arrival times of S- and P-waves of about 1 s at INS1 station. The average depth retrieved from preliminary earthquake location analyses is about 4.5 km and the maximum recorded local magnitude is Ml = 1.4, related to an earthquake occurred on 2018-01-29 at

15:23:10 UTC, located at about 1.4 km epicentral distance from INS1 station with focal depth of about 3.50 km (Figure 9a). Most of detected IIE have a magnitude lower than 1; only four of them are characterized by local magnitude 1<Ml≤1.4. Depending on the earthquake energy, the number of stations that recorded the seismic signals changes from a minimum of 3 for the lowest magnitude event up to 16, taking into account also stations belonging to the virtual seismic network. The waveforms, usually, have duration less than 7 s at the closest station (INS1) and the highest peak ground velocity amplitude (PGV) measured at that station is about 0.04 mm s^{-1} for to the strongest IIE of the catalogue (Figure 9a).

b) RIE: a total number of 116 reservoir-induced seismic events was manually detected, in the range Ml = 0 – 1.8. The P-wave arrivals are usually first detected at either INS5 or INS6 or INS7 seismic station, depending on the earthquake location: indeed, such seismic events belong to a wider cluster than IIE one and therefore they are more broadly distributed in the southwestern part of the seismic network (Figure 1). Their average depth is about 4.5 km and the maximum recorded local magnitude is Ml = 1.8, related to an earthquake occurred on 2017-03-02 at 21:39:41 UTC, located at about 1.9 km epicentral distance from INS5 station with focal depth of about 5.45 km (Figure 9b). Because of the proximity of the stations around this seismicity cluster, also RIE earthquakes, in a way similar to IIE, are characterized by a difference between S- and P-wave arrival times of about 1 s at the closest station to the epicenter and short duration, less than 8 s (e.g. see Figure 9b). The recorded seismic event with lowest magnitude was detected by 7 stations, whereas the strongest earthquake was recorded by 12 stations. Finally, the highest peak ground velocity amplitude recorded up to now for this earthquake category is about 0.08 mm s^{-1} (Figure 9b).

c) LE: a total number of 698 local natural earthquakes has been detected. The main difference with respect to the IIE and RIE is their higher average hypocentral depths, that is about 10 km depth, more similar to the typical depth of Apennines crustal earthquakes. Most of recorded LE are characterized by a local magnitude < 2: indeed, only 21 seismic events out of 388 have greater magnitude. Three earthquakes with a magnitude greater than 3, included in a radius of about 40 km from the center of INSIEME seismic network, have been recorded. The strongest event is a Mw = 3.8 earthquake, 14 km depth, which occurred about 5 km distance from the closest seismic station to the epicenter, that is MTSN, managed by INGV: at this receiver, the highest peak ground velocity amplitude of more than 3 mm s^{-1} was recorded. This event was detected by the whole INSIEME seismic network, as well as by all the stations of the virtual network that were in operation that day; in Figure 10 the vertical components of the 18 stations that have recorded the event are displayed.

Concerning teleseismic events, the INSIEME network was able to record the most energetic earthquakes occurred worldwide in the period in which the analyses have been carried out. In Figure 11, the recordings at INS1 station of seismic waves generated by the Mw=7.6 Chile earthquake of 2016-12-25 are shown. We specifically choose to display the waveforms at INS1 station since it was installed at 50 m depth and it is a 120 s instrument: these elements allowed to clearly see the most important seismic phases generated by the earthquake and by the effects of propagation inside the Earth. Their theoretical arrival times were computed by means of Seisgram2k software (Lomax, 2008) which uses the Preliminary Reference Earth Model (PREM) published by Dziewonsky and Anderson (1981). In addition to different seismic phases, in Figure 11 we are able to observe the different frequency components of surface waves: the lower frequencies, travelling deeper in the Earth and, therefore, faster, arrive at INS1 station before the components characterized by higher frequencies.

4 Data availability

The INSIEME network has been registered at the International Federation of Digital Seismograph Networks (FDSN), which assigned to such temporary experimental network the code 3F. Open-access policy on these data has been adopted and they are available from http://www.fdsn.org/networks/detail/3F_2016 (https://doi.org/10.7914/SN/3F_2016; Stabile et al., 2016). At the end of the SIR-MIUR INSIEME project (2019-03-23), we have decided to do not uninstall the network and we are going to update it as a permanent open-access seismic network.

5 Discussion and conclusions

In this paper we have presented the data collected by the INSIEME seismic network deployed in the HAV to feed the research activities of the SIR-MIUR INSIEME project with new high-quality seismic data. Beyond the research purposes of the INSIEME project, we have adopted open-access policy on the continuous data streams acquired by the seismic network since the begin of data acquisition with the aim to share with the whole scientific community data collected in a very attractive area where both natural and induced events are observed. In this sense, the network can be considered as an open-access research infrastructure for studying induced seismicity processes and for developing methodologies for discriminating between natural and induced earthquakes.

All the 8 stations of the network are equipped with broadband sensors, consisting in six 20s-100Hz Trillium Compact Posthole and two 120s-100Hz Trillium Compact Posthole, installed in PVC casings at different depths down to 50 m. The power supply of stations is provided by solar panels and batteries. Only INS1 station was initially connected to a power line, but on 2018-04-14 at 19:16:57 UTC the electric power grid of the Montemurro Cemetery (which powered the station) started to have troubles, thus resulting as a disturbance on the seismic signal. After several attempts the problem was definitively by-passed on 2018-06-29, between 7:19 and 10:04 UTC by connecting also this station to a power system based on solar panels and batteries. The quality of acquired data has been investigated for each station in terms of both the background noise level and the local ground effects. Our analyses indicate that the installation of sensors in PCV casing at 6 m depth allows a reduction of the noise level up to 20 dB with respect to the noise level recorded at surface and that there is not a significant difference of the noise level recorded between 6 and 50 m depth. Furthermore, all the stations are installed on sites with negligible amplification, except station INS5 where a small amplification is observed at about 3.5 Hz (Figure 8).

Between September 2016 and December 2018 we have manually detected 856 local natural and induced earthquakes, which were preliminarily located with the Origin Locator Viewer (scolv) tool of the software SeisComP3 running on the server of the INSIEME network: 42 events (Ml≤1.4) are classified as IIE, 116 events are (Ml≤1.8) classified as RIE, and 698 events (Ml≤3.8) are LE. The availability of a continuous data stream will give the advantage to apply robust automated data analysis procedures for earthquake detection and location such as the master-event waveform stacking method (Grigoli et al., 2016), the multiband array detection and location method (Poiata et al., 2016), template matching algorithms (e.g., Gibbons and Ringdal, 2006), or to develop and test new algorithms. As an example, we are developing a template-matching algorithm and

https://doi.org/10.5194/essd-2019-113
Preprint. Discussion started: 5 July 2019

we performed a first test by using some IIE recorded at INS1 station as event templates, obtaining additional 135 detections of IIE. In this way it is possible to lower the detection threshold of the seismic network and, consequently, to decrease the magnitude of completeness which leads to the production of a larger microseismic catalog.

These new seismicity data, hopefully incremented with recordings coming from the stations of the virtual network, could be used for further seismological studies, such as seismic tomographies (both elastic and anelastic), focal mechanisms and estimation of source parameters of each individual event, detailed earthquake locations to study the space-time evolution of seismicity and for fault imaging, and seismic hazard analyses for a better comprehension of the seismic potential of the area.

Besides IIE, RIE and LE categories, continuous acquisition allowed to record teleseisms that occurred worldwide. These data acquired by the broad-band sensors of the INSIEME network could integrate the data collected by the Global Seismographic Network (GNS, https://earthquake.usgs.gov/monitoring/gsn, last access: June 2019) or by the GEOFON global seismological broad-band network (https://geofon.gfz-potsdam.de, last access: June 2019) for real-time global earthquake monitoring or for global seismology studies. The great coherence of teleseismic recordings provided by such a dense seismic network can be used also as an antenna to track the energy radiated by the propagating rupture along a fault (e.g., Satriano et al., 2014) or, more generally, for seismic array applications (e.g., Gibbons et al., 2008).

In addition to the applications mentioned above, all based on earthquake recordings, continuous data streams provide also large datasets of noise data to be processed for obtaining broad-band surface waves dispersion curves (Bensen et al., 2007), which could be adopted for ambient noise tomographies of the study area (Shapiro et al., 2005).

Finally, it is important to highlight that the INSIEME seismic network will continue to operate also after the end of the SIR-MIUR INSIEME project (2019-03-23) by becoming an open-access permanent seismic network of the High Agri Valley geophysical Observatory (HAVO) managed by the CNR-IMAA research institute.

Author contributions. TAS led the writing of the paper and VS prepared sections 3.2 and 3.3. TAS and CS worked on the seismic network layout and on the choice of the acquisition system. MR installed sensors in PVC casing at different depths and evaluated boreholes inclination. TAS evaluated sensors orientation and signal quality in terms of noise level. JMS and ER organized the CNR-IMAA Data Center, including real-time data transmission from the remote stations to the Data Center and the installation of softwares for data processing. EG and TAS performed geological surveys and verified the access to the site, the data transmission conditions and unexpected potential sources of local noise. HVSR and HVNSR analyses where performed by VS and MRG. TAS, VS, JB and SP manually picked the seismic phases and located the natural and anthropogenic seismic events. All co-authors provided comments which contributed to the paper.

Competing interests. The authors declare that they have no conflict of interest.

Acknowledgements. The authors would like to thank the mayors of the municipalities that host the seismic stations of the INSIEME network for their authorizations: Senatro Di Leo (Montemurro), Cesare Marte (Sarconi), Antonio Maria Imperatrice

(Grumento Nova), Amedeo Cicala (Viggiano), Franco Curto (Armento), and Mario Solimando (Spinoso). Figures 1, 5, 6, and 7 were drawn using Matplotlib (Hunter, 2007) and ObsPy (Beyreuther et al., 2010) python libraries. Figures 9, 10, and 11 were drawn using the Seismic Analysis Code (Goldstein et al., 2003).

Financial support. This work has been funded by the INSIEME project of the Italian SIR-MIUR program (grant no. RBSI14MN31).

References

Beauducel, F., Bosson, A., Randriamora, F., Anténor-Habazac, C., Lemarchand, A., Saurel, J.-M., Nercessian, A., Bouin, M. P., de Chabalier, J. B., and Clouard, V.: Recent advances in the Lesser Antilles observatories - Part 2 — WEBOBS: An integrated web-based system for monitoring and networks management, EGU General Assembly, Geophys. Res. Abstr., 12, EGU2010-5098, 2010.

Bensen, G. D., Ritzwoller, M. H., Barmin, M. P., Levshin, A. L., Lin, F., Moschetti, M. P., Shapiro, N. M., and Yang, Y.: Processing seismic ambient noise data to obtain reliable broad-band surface wave dispersion measurements, Geophys. J. Int., 169(3), 1239–1260, https://doi.org/10.1111/j.1365-246X.2007.03374.x, 2007.

Beyreuther, M., Barsch, R., Krischer, L., Megies, T., Behr, Y., and Wassermann, J.: ObsPy: A Python Toolbox for Seismology, Seismol. Res. Lett., 81(3), 530-533, https://doi.org/doi:10.1785/gssrl.81.3.530, 2010.

Burrato, P., and Valensise, G.: Rise and Fall of a Hypothesized Seismic Gap: Source Complexity in the Mw 7.0 16 December 1857 Southern Italy Earthquake, Bull. Seismol. Soc. Am., 98(1), 140–144, https://doi.org/10.1785/0120070094, 2008.

Dziewonsky, A. M., and Anderson, D. L. : Preliminary Earth Reference Model, Phys. Earth Planet. Inter., 25(4), 297–356, https://doi.org/10.1016/0031-9201(81)90046-7, 1981.

Ellsworth, W. L.: Injection-induced earthquakes, Science, 341(6142), 1225942, https://doi.org/10.1126/science.1225942, 2013.

Foulger, G. R., Wilson, M. P., Gluyas, J. G., Julian, B. R., and Davies R. J.: Global review of human-induced earthquakes, Earth-Sci. Rev., 178, 438–514,. https://doi.org/10.1016/j.earscirev.2017.07.008, 2018.

Gibbons, S. J., and Ringdal, F.: The detection of low magnitude seismic events using array-based waveform correlation, Geophys. J. Int., 165(1), 149–166, https://doi.org/10.1111/j.1365-246X.2006.02865.x, 2006.

Gibbons, S. J., Ringdal, F., and Kværna, T.: Detection and characterization of seismic phases using continuous spectral estimation on incoherent and partially coherent arrays, Geophys. J. Int., 172(1), 405–421, https://doi.org/10.1111/j.1365-246X.2007.03650.x, 2008.

Giocoli, A., Stabile, T. A., Adurno, I., Perrone, A., Gallipoli, M. R., Gueguen, E., Norelli, E., and Piscitelli, S.: Geological and geophysical characterization of the south-eastern side of the High Agri Valley (southern Apennines, Italy), Nat. Haz. Earth Sys. Sci., 15(2), 315–323, https://doi.org/10.5194/nhess-15-315-2015, 2015.

Grigoli, F., Cesca, S., Krieger, L., Kriegerowski, M., Gammaldi, S., Horalek, J., and Dahm, T.: Automated microseismic event location using Master-Event Waveform Stacking, Sci. Rep., 6, 25744, https://doi.org/10.1038/srep25744, 2016.

Grigoli, F., Cesca, S., Priolo, E., Rinaldi, A. P., Clinton, J. F., Stabile, T. A., Dost, B., Fernandez, M. G., Wiemer, S., and Dahm, T.: Current challenges in monitoring, discrimination, and management of induced seismicity related to underground industrial activities: A European perspective, Rev. Geophys., 55(2), 310–340, https://doi.org/10.1002/2016RG000542, 2017.

Goldstein, P., Dodge, D., Firpo, M., and Minner L.: SAC2000: Signal processing and analysis tools for seismologists and engineers, in: The IASPEI International Handbook of Earthquake and Engineering Seismology, edited by: Lee, W. H. K. et al., Academic Press, London, 2003.

Gruppo di Lavoro MPS: Redazione della mappa di pericolosità sismica prevista dall'Ordinanza PCM 3274 del 20 marzo 2003, Rapporto Conclusivo per il Dipartimento della Protezione Civile, INGV, Milano-Roma, 65 pp., 2004.

Havskov, J., Ottemöller, L., Trnkoczy, A., and Bormann, P.: Seismic Networks, in: New Manual of Seismological Observatory Practice (NMSOP-2), IASPEI, edited by: Bormann, P., GFZ German Research Centre for Geosciences, Ch.8, 65 pp., https://doi.org/10.2312/GFZ.NMSOP-2_CH8, 2012.

Hunter, J. D.: Matplotlib: A 2D graphics environment, IEEE Comput. Sci. Eng. 9(3), 90–95, https://doi.org/10.1109/MCSE.2007.55, 2007.

Hutt, C. R., Ringler, A. T., and Gee, L. S.: Bull. Broadband seismic noise attenuation versus depth at the Albuquerque Seismological Laboratory, Bull. Seismol. Soc. Am., 107(3), 1402–1412, https://doi.org/10.1785/0120160187, 2017.

Improta, L., Valoroso, L., Piccinini, D., and Chiarabba, C.: A detailed analysis of wastewater-induced seismicity in the Val d'Agri oil field, Italy, Geophys. Res. Lett., 42(8), 2682–2690, https://doi.org/10.1002/2015GL063369, 2015.

Improta, L., Bagh, S., De Gori, P., Valoroso, L., Pastori, M., Piccinini, D., and Buttinelli, M.: Reservoir structure and wastewater-induced seismicity at the Val d'Agri oilfield (Italy) shown by three-dimensional Vp and Vp/Vs local earthquake tomography, J. Geophys. Res. Solid Earth, 122(11), 9050–9082, https://doi.org/10.1002/2017JB014725, 2017.

Keranen, K. M., and Weingarter, M.: Induced Seismicity, Annu. Rev. Earth Planet. Sci., 46(1), 149–174, https://doi.org/10.1146/annurev-earth-082517-010054, 2018.

Konno, K., and Ohmachi, T.: Ground-motion characteristic estimated from spectral ratio between horizontal and vertical components of micro-tremor, Bull. Seismol. Soc. Am., 88(1), 228–241, 1998.

Lee, K.-K., Ellsworth, W. L., Giardini, D., Townend, J., Ge, S., Shimamoto, T., Yeo, I.-W., Kang, T.-S., Rhie, J., Sheen, D.-H., Chang, C., Woo, J.-U., Langenbruch, C.: Managing injection-induced seismic risks, Science, 364(6442), 730-732, https://doi.org/10.1126/science.aax1878, 2019.

Lee, W. H. K., and Lahr, J. C.: HYPO71 (revised): A Computer Program for Determining Hypocenter, Magnitude, and First Motion Pattern of Local Earthquakes, Geol. Surv., Open-File Rep. (U.S.) 116 pp, 75–311, 1972.

Lentas, K., Di Giacomo, D., Harris, J., and Storchak, D. A.: The ISC Bulletin as a comprehensive source of earthquake source mechanisms, Earth Syst. Sci. Data, 11, 565-578, https://doi.org/10.5194/essd-11-565-2019, 2019.

Longuet-Higgins, M. S.: A theory of the origin of microseisms. Phil. Trans. Roy. Soc. Lond., 243(857), 1-35, 1950.

https://doi.org/10.5194/essd-2019-113
Preprint. Discussion started: 5 July 2019

Lomax, A., Virieux, J., Volant, P., and Berge, C.: Probabilistic earthquake location in 3-D and layered models: Introduction of a Metropolis-Gibbs method and comparison with linear locations, in: Advances in seismic event location, edited by: Thurber, C. H., and Rabinowitz, N., Amsterdam, Kluwer, 101–134, 2000.

Lomax, A: SeisGram2K-Seismogram visualization and analysis software for the Internet-Ver5.3, http://alomax.free.fr/seisgram/SeisGram2K.html, last access: June 2014, 2008.

Mallet, R.: The great Neapolitan earthquake of 1857. The first principles of observational seismology, Chapman and Hill, London, England, vol. I, 431 pp., vol. II, 399 pp., 1862.

McGarr, A.: Maximum magnitude earthquakes induced by fluid injection, J. Geophys. Res. Solid Earth, 119(2), 1008–1019, https://doi.org/10.1002/2013JB010597, 2014.

McNamara, D. E., and Buland, R. P.: Ambient noise levels in the continental United States, Bull. Seismol. Soc. Am., 94(4), 1517-1527, https://doi.org/10.1785/012003001, 2004.

Nakamura, Y.: A method for dynamic characteristics estimation of subsurface using microtremor on the ground surface, Quart. Rep. Jpn. Railway Tech. Res. Inst. (RTRI), 30(1), 25–33, 1989.

National Research Council: Induced Seismicity Potential in Energy Technologies, The National Academies Press, Washington, D. C., 262 pp., 2013.

Patacca, E, and Scandone, P.: Post-Tortonian mountain building in the Apennines: The role of the passive sinking of a relic lithospheric slab, in: The lithosphere in Italy: advances in earth science research, edited by: Boriani A., et al., Atti Conv. Lincei, 80, 157–176, 1989.

Peterson, J.: Observations and Modeling of Seismic Background Noise, U.S. Geological Survey Open-File Report 93-322, 1993.

Poiata, N., Satriano, C., Vilotte, J. P., Bernard, P., and Obara, K.: Multiband array detection and location of seismic sources recorded by dense seismic networks, Geophys. J. Int., 205(3), 1548–1573, https://doi.org/10.1093/gji/ggw071, 2016.

Pratt, W. E., and D. W. Johnson: Local subsidence of the Goose Creek oil field (Texas), Bull. Seismol. Soc. Am., 34(7), 577–590, 1926.

Priolo, E., Romanelli, M., Plasencia Linares, M. P., Garbin, M., Peruzza, L., Romano, M. A., Marotta, P. Bernardi, P., Moratto, L., and D. Zuliani, D.: Seismic monitoring of an underground natural gas storage facility: The Collalto Seismic Network, Seismol. Res. Lett., 86(1), 109–123, https://doi.org/10.1785/0220140087, 2015.

Rovida, A., Camassi, R., Gasperini, P., and Stucchi, M.: CPTI11, la versione 2011 del catalogo Parametrico dei Terremoti Italiani, INGV, Milano, Bologna, Italy, https://doi.org/10.6092/INGV.IT-CPTI11, 2011.

Satriano, C., Dionicio, V., Miyake, H., Uchida, N., Vilotte, J.-P., and Bernard, P.: Structural and thermal control of seismic activity and megathrust rupture dynamics in subduction zones: Lessons from the Mw 9.0, 2011 Tohoku earthquake, Earth Planet. Sci. Lett., 403, 287-298, https://doi.org/10.1016/j.epsl.2014.06.037, 2014.

Serlenga, V., and Stabile, T. A.: How do Local Earthquake Tomography and inverted dataset affect earthquake locations? The case study of High Agri Valley (Southern Italy), Geomat. Nat. Haz. Risk, 10(1), 49-78, https://doi.org/10.1080/19475705.2018.1504124, 2019.

Spriggs, N., Bainbridge, G., and Greig, W.: Comparison study between vault seismometers and posthole seismometers, EGU General Assembly, Geophys. Res. Abstr., 16, EGU2014-6441, 2014.

Stabile, T. A., Iannaccone, G., Zollo, A., Lomax, A., Ferulano, M. F., Vetri, M. L. V., and Barzaghi, L. P.: A comprehensive approach for evaluating network performance in surface and borehole seismic monitoring, Geophys. J. Int., 192(2), 793–806, https://doi.org/10.1093/gji/ggs049, 2013.

Stabile, T. A., Giocoli, A., Lapenna, V., Perrone, A., Piscitelli, S., and Telesca, L.: Evidences of low-magnitude continued reservoir-induced seismicity associated with the Pertusillo artificial lake (southern Italy), Bull. Seismol. Soc. Am., 104(4), 1820–1828, https://doi.org/ 10.1785/0120130333, 2014a.

Stabile, T. A., Giocoli, A., Perrone, A., Piscitelli, S., and Lapenna, V.: Fluid injection induced seismicity reveals a NE dipping fault in the southeastern sector of the High Agri Valley (southern Italy), Geophys. Res. Lett., 41, 5847–5854, https://doi.org/10.1002/2014GL060948, 2014b.

Stabile, T. A., Giocoli, A., Perrone, A., Piscitelli, S., Telesca, L., and Lapenna, V.: Relationship between seismicity and water level of the Pertusillo reservoir (southern Italy), Boll. Geof. Teor. Appl., 56(4), 505–517, https://doi.org/10.4430/bgta0161, 2015.

Stabile T. A., and the INSIEME Team: SIR-MIUR Project INSIEME - broadband seismic network in Val d'Agri (southern Italy), International Federation of Digital Seismograph Networks, Dataset/Seismic Network, https://doi.org/10.7914/SN/3F_2016, 2016.

Shapiro, N. M., Campillo, M., Stehly, L., and Ritzwoller, M. H.: High-Resolution Surface wave Tomography from Ambient Seismic Noise, Science, 307(5715), 1615-1618, https://doi.org/10.1126/science.1108339, 2005.

Telesca, L., Giocoli, A., Lapenna, V., and Stabile, T. A.: Robust identification of periodic behavior in the time dynamics of short seismic series: the case of seismicity induced by Pertusillo Lake, southern Italy, Stoc. Environm. Res. Risk Asses., 29(5), 1437–1446, https://doi.org/10.1007/s00477-014-0980-6, 2015.

Valoroso, L., Improta, L., Chiaraluce, L., Di Stefano, R., Ferranti, L., Govoni, A., and Chiarabba, C.: Active faults and induced seismicity in the Val d'Agri area (southern Apennines, Italy), Geophys. J. Int., 178, 488–502. https://doi.org/10.1111/j.1365-246X.2009.04166.x, 2009.

Vlček, J., Eisner, L., Stabile, T. A., and Telesca, L.: Temporal relationship between injection rates and induced seismicity, Pure Appl. Geophys., 175(8), 2821–2835, https://doi.org/10.1007/s00024-017-1622-y, 2018.

Weber, E., Convertito, V., Iannaccone, G., Zollo, A., Bobbio, A., Cantore, L., Corciulo, M., Di Crosta, M., Elia, L., Martino, C., Romeo, A., and Satriano, C.: An Advanced Seismic Network in the Southern Apennines (Italy) for Seismicity Investigations and Experimentation with Earthquake Early Warning, Seism. Res. Lett. 78(6), 622-634, https://doi.org/10.1785/gssrl.78.6.622, 2007.

Wcisło, M., Stabile, T. A., Telesca, L., and Eisner, L.:. Variations of attenuation and Vp/Vs ratio in the vicinity of wastewater injection: a case study of Costa Molina 2 well (High Agri Valley, Italy), Geophysics, 83(2), B25–B31, https://doi.org/10.1190/GEO2017-0123.1, 2018.

Withers, M. M., Aster, R. C., Young, C. J., and Chael, E. P.: High-frequency analysis of seismic background noise as a function of wind speed and shallow depth, Bull. Seismol. Soc. Am., 86(5), 1507–1515, 1996.

Young, C. J., Chael, E. P., Zagar, D. A., and Carter, J. A.: Variations in noise and signal levels in a pair of deep boreholes near Amarillo, Texas, Bull. Seismol. Soc. Am., 84(5), 1593–1607, 1994.

Zheng, X., and McMechan, G. A.: Two methods for determining geophone orientations from VSP data, Geophysics, 71(4), V87–V97, 2006.

Tables

Table 1: Geographic coordinates and elevation of the INSIEME broadband seismic stations with indication of the sensor type installed at each station (TCP = Trillium Compact Posthole).

Station name	Latitude °N	Longitude °E	Elevation (m a.s.l.)	Sensor type
INSX	40.305686	15.989105	806	20s-100Hz TCP
INS1	40.305790	15.988603	802	120s-100Hz TCP
INS2	40.342090	15.951559	1043	20s-100Hz TCP
INS3	40.328033	16.034446	880	20s-100Hz TCP
INS4	40.278168	16.040405	652	20s-100Hz TCP
INS5	40.275704	15.906211	602	20s-100Hz TCP
INS6	40.229581	15.887608	745	20s-100Hz TCP
INS7	40.221487	15.917465	881	120s-100Hz TCP
INS8	40.241083	15.972221	882	20s-100Hz TCP

Table 2: Position of the broadband sensors during time for each station with the indication of the sensor depth when it is installed in the borehole.

Station name	surface		borehole		Sensor depth
	installation	uninstallation	installation	uninstallation	

https://doi.org/10.5194/essd-2019-113
Preprint. Discussion started: 5 July 2019

Open Access Earth System Science Data Discussions

INSX	2016-04-01	2017-01-24	-	-	-
INS1	-	-	2016-10-12	-	50 m
INS2	2016-09-23	2017-03-22	2017-03-22	-	6 m
INS3	2016-08-26	2017-03-22	2017-03-22	-	6 m
INS4	2016-08-26	2017-03-22	2017-03-22	-	6 m
INS5	2016-08-26	2016-10-13	2016-10-13	-	6 m
INS6	2016-08-26	2017-03-22	2017-03-22	-	6 m
INS7	2017-03-02	2017-03-23	2017-03-23	-	14 m
INS8	2017-03-02	-	-	-	-

Figures

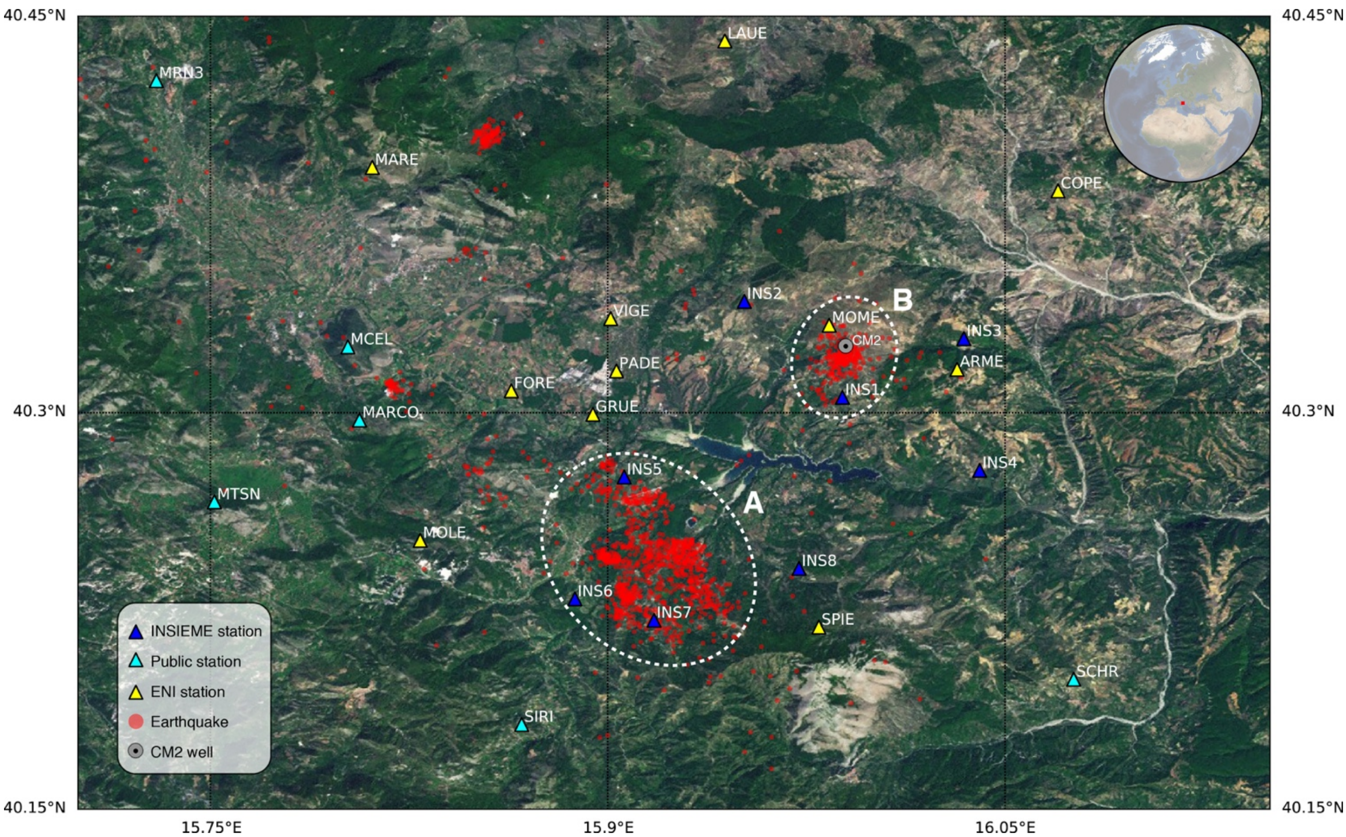

https://doi.org/10.5194/essd-2019-113
Preprint. Discussion started: 5 July 2019

Open Access Earth System Science Data Discussions

Figure 1: Layout of the INSIEME seismic network in the High Agri Valley. Blue triangles represent the 8 broadband seismic stations of the network. Yellow and cyan triangles represent stations belonging to private (i.e. the Eni Company) and public seismic monitoring networks, respectively. The CM2 injection well is depicted with a black dot inside a grey circle. Natural and anthropogenic earthquakes are represented with red circles. Anthropogenic seismicity is classified as continued reservoir (clusters A) and fluid-injection (cluster B) induced seismicity. The map was drawn using Matplotlib python library (Hunter, 2007) which incorporates the ArcGIS REST Services freely available at http://server.arcgisonline.com/arcgis/rest/services.

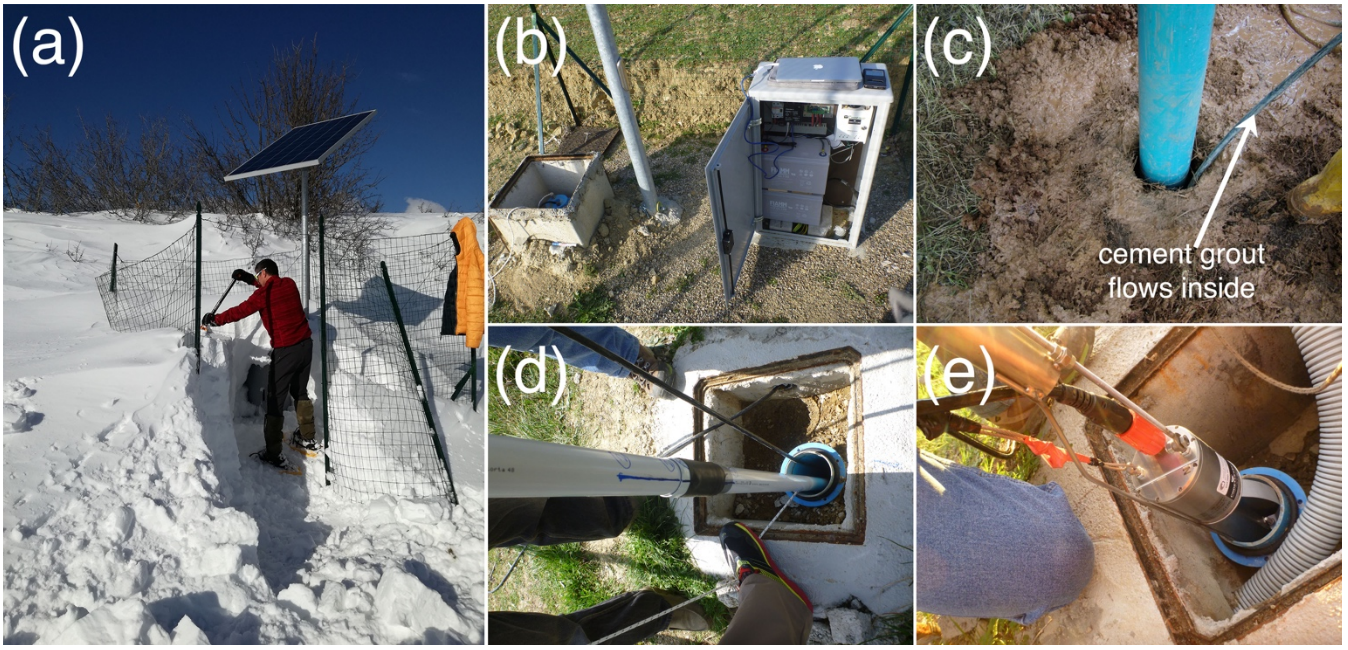

Figure 2: Details of a typical seismic station of the INSIEME network: (a) the solar panel is installed on a pole of 2 m height in order to prevent that it is covered by snow during the Winter season; (b) all the instruments of a station are housed in a small cabin which is connected to the borehole where the seismometer is installed inside a PVC casing; (c) the PVC casing is coupled to the soil by using a cement grout; (d) the PVC casing is not centered in order to leave space for installing sensors on the surface and seismometers placed at 6 m depth are installed by using a non-rotating arm; (e) all the broadband seismometers installed in boreholes are equipped with a coupling system.

https://doi.org/10.5194/essd-2019-113
Preprint. Discussion started: 5 July 2019

Open Access Earth System Science Data Discussions

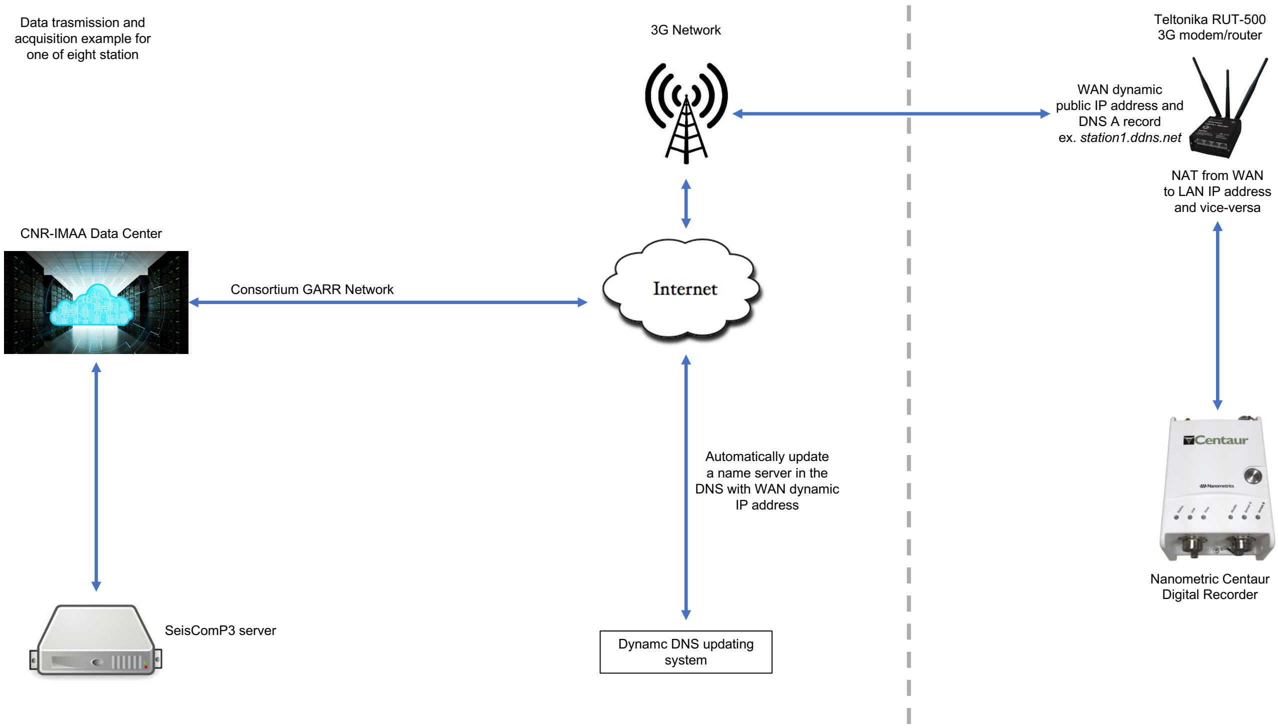

Figure 3: Schematic view of the data flow from the data-logger of a remote station to the CNR-IMAA Data Centre.

https://doi.org/10.5194/essd-2019-113
Preprint. Discussion started: 5 July 2019

Earth System Science Data
Open Access Discussions

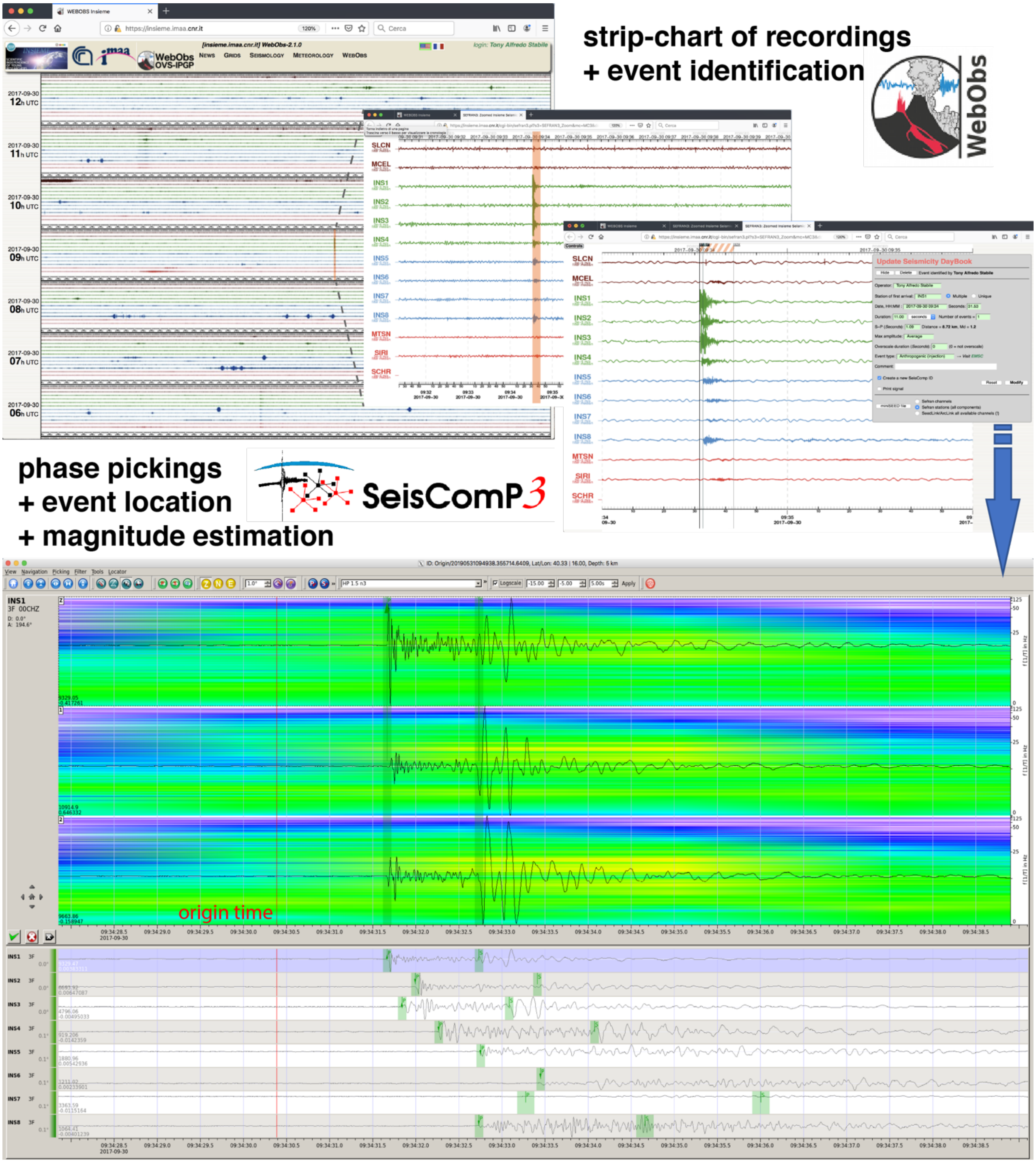

5 **Figure 4: Tools implemented for visualization and processing of acquired seismic data. The WebObs intranet system (top panels) is used to plot in near real-time strip-chart of recordings at configured stations any event present in the data. When an event is identified, the information is sent to the SeisComP3 database for the manual phase picking and event location (bottom panel) through the Origin Locator Viewer tool (scolv).**

https://doi.org/10.5194/essd-2019-113
Preprint. Discussion started: 5 July 2019

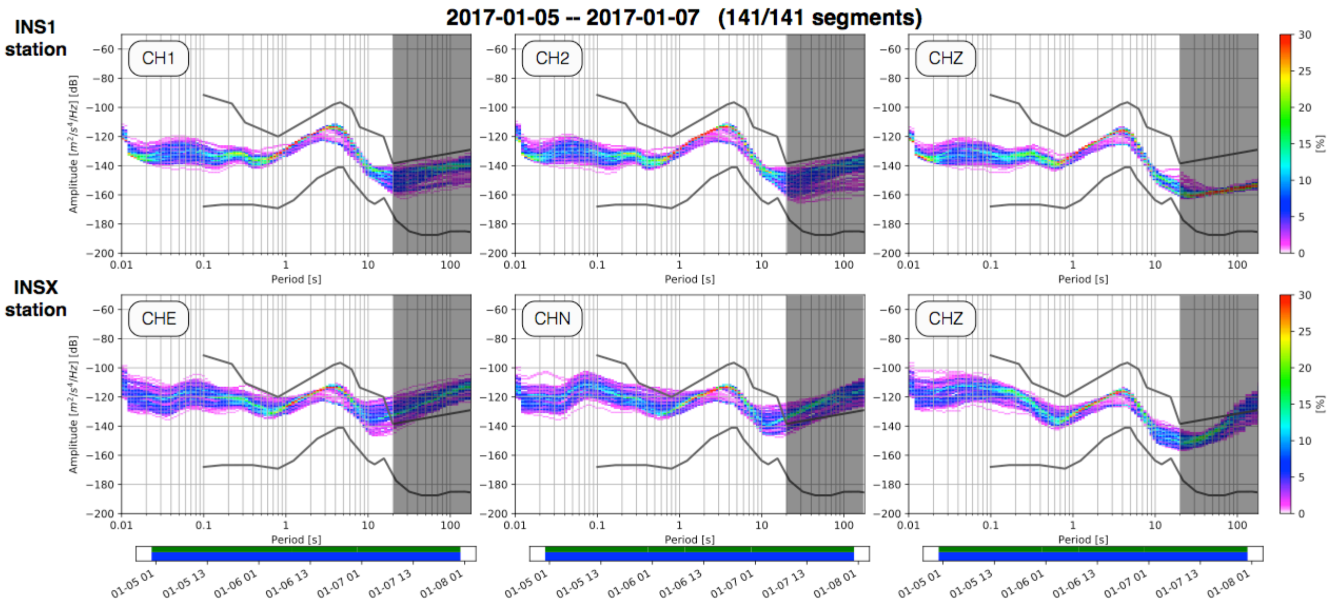

Figure 5: PPSD computed for each component of station INS1 (top panels), with sensor installed at 50 m depth, and station INSX (bottom panels), with sensor installed at surface. The colour palette indicates the probability (in percentage) to have a certain noise level. The two grey lines in each panel indicate the High and Low Noise models, respectively, obtained by Peterson (1993). Below each actual PPSD there is visualized the data basis for the PPSD. The top row shows data fed into the PPSD: green patches represent available data, red patches (not in this case) represent eventual gaps in streams. The bottom row in blue shows the single PSD measurements that go into the histogram. Periods above 20 s are highlighted in grey because in such period range it is not possible to compare the PPSD of the two stations (only the sensor of INS1 stations has flat response up to 120 s).

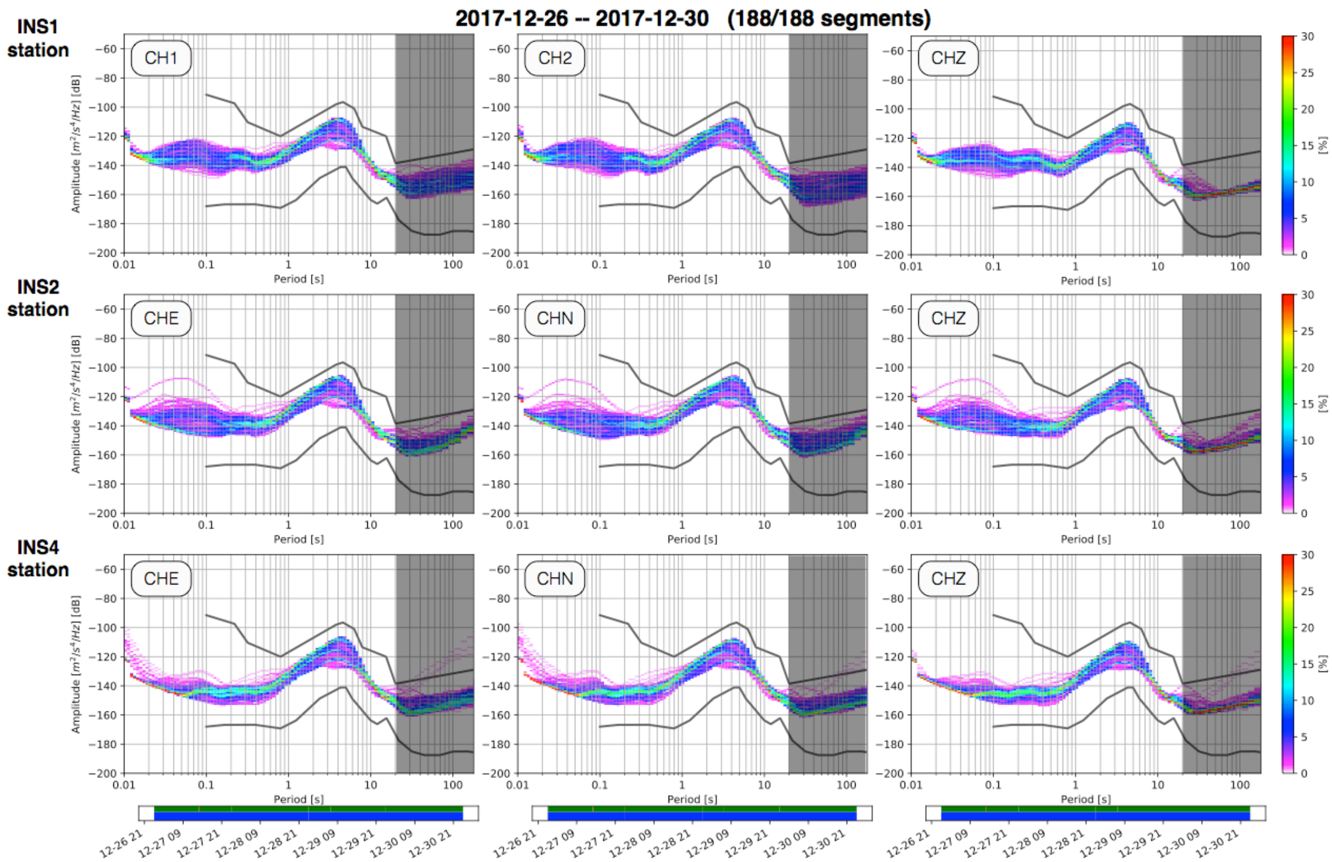

Figure 6: Same type of comparison as Figure 5 but among stations INS1 (sensor installed at 50 m depth), INS2 and INS4 (respective sensors both installed at 6 m depth).

https://doi.org/10.5194/essd-2019-113
Preprint. Discussion started: 5 July 2019

Open Access Earth System Science Data Discussions

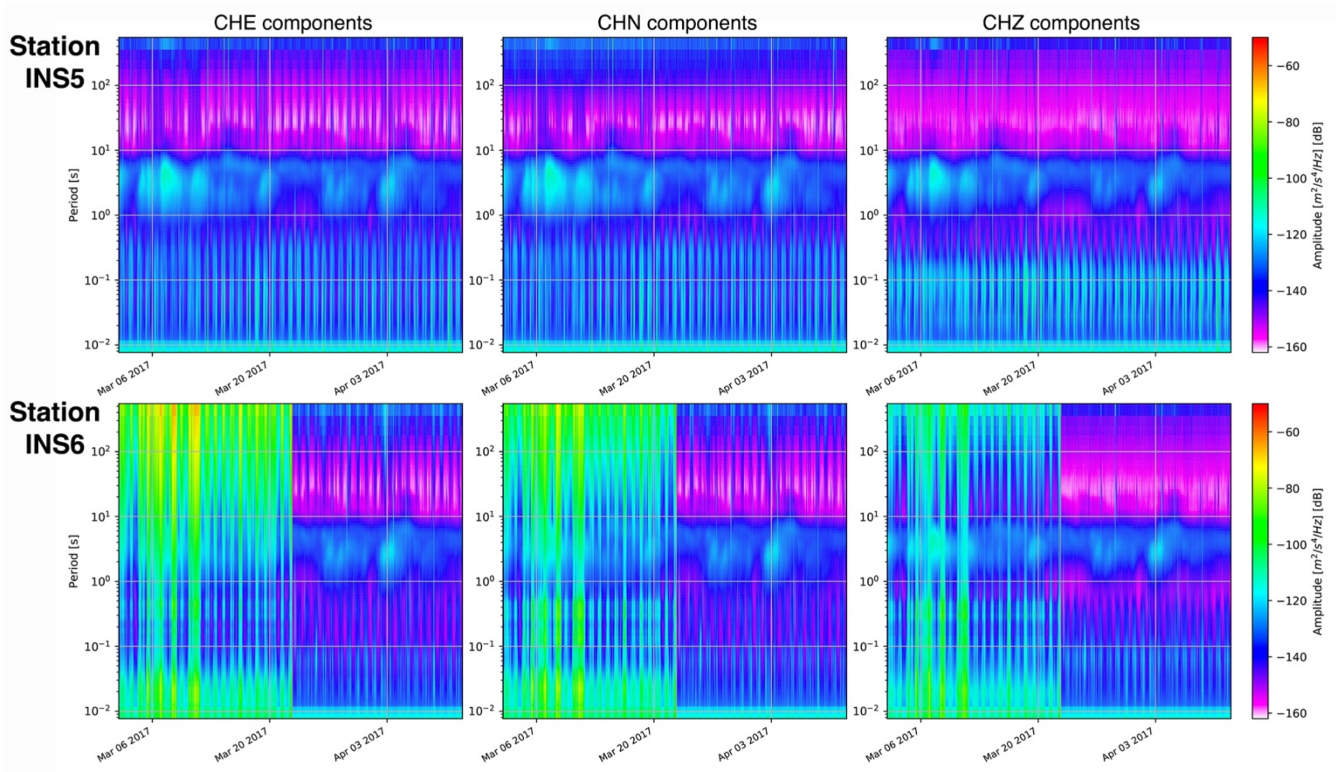

Figure 7: Spectrograms of each component of station INS5 (top panels) and INS6 (bottom panels) computed over continuous data streams of 41 days (from 2017-03-02 to 2017-04-11). The sensor of station INS5 was installed at 6 m depth for the whole period of observation whereas the sensor of station INS6 was first installed on surface and then moved at 6 m depth on 2017-03-22.

https://doi.org/10.5194/essd-2019-113
Preprint. Discussion started: 5 July 2019

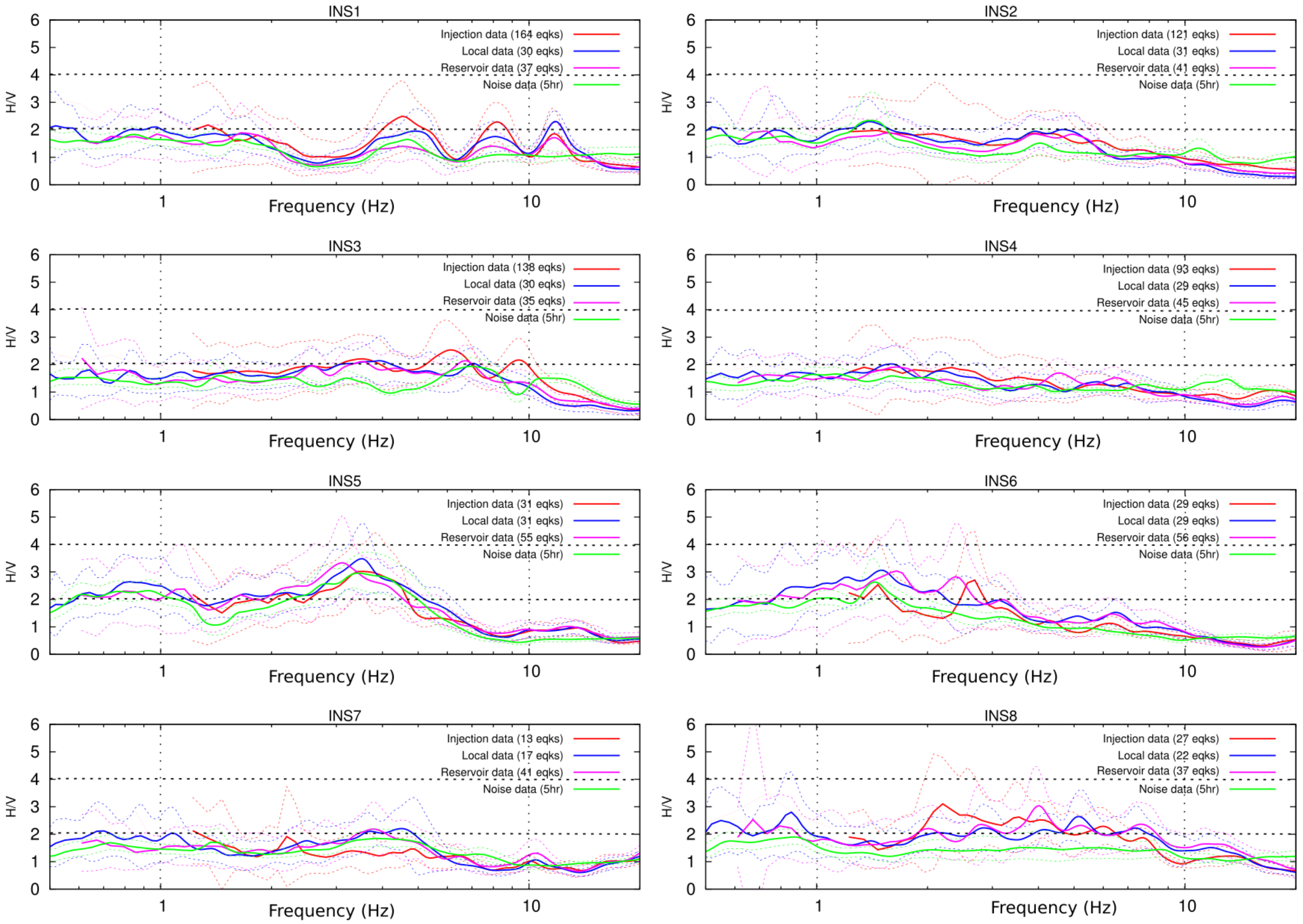

Figure 8: HVSR and HVNSR curves computed at all the INSIEME network seismic stations. For each dataset, the number of used earthquakes and the hours of seismic noise are indicated. The solid coloured line represent the average HVSR and HVNSR curves, whereas the dashed lines identify the ±1σ standard deviations.

https://doi.org/10.5194/essd-2019-113
Preprint. Discussion started: 5 July 2019

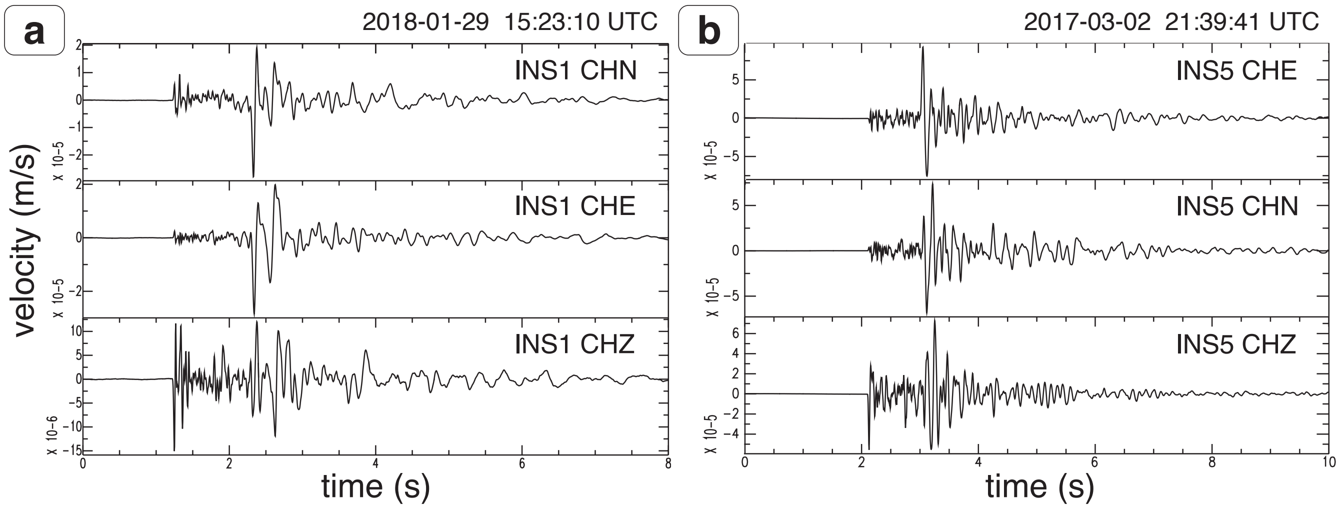

Figure 9: (a) The largest injection induced earthquake (Ml=1.4, Lat=40.3182˚N, Lon=15.9842˚E, depth=3.50 km) recorded by the INS1 seismic station at 1.4 km epicentral distance, and (b) the largest reservoir induced earthquake (Ml=1.8, Lat=40.2700˚N, 15.8848˚E, depth=5.45 km) recorded by the INS5 seismic station at 1.9 km epicentral distance. On the top of the figures the seismic event origin time is reported. For station INS1 the original horizontal components were rotated counter-clockwise by an angle of 307.8° with respect to the North, according to the computations described in detail in section 2.2. A Ts – Tp of about 1 s can be clearly noticed for both the injection and the reservoir induced events at the correspondent closest station.

https://doi.org/10.5194/essd-2019-113
Preprint. Discussion started: 5 July 2019

Open Access Earth System Science Data Discussions

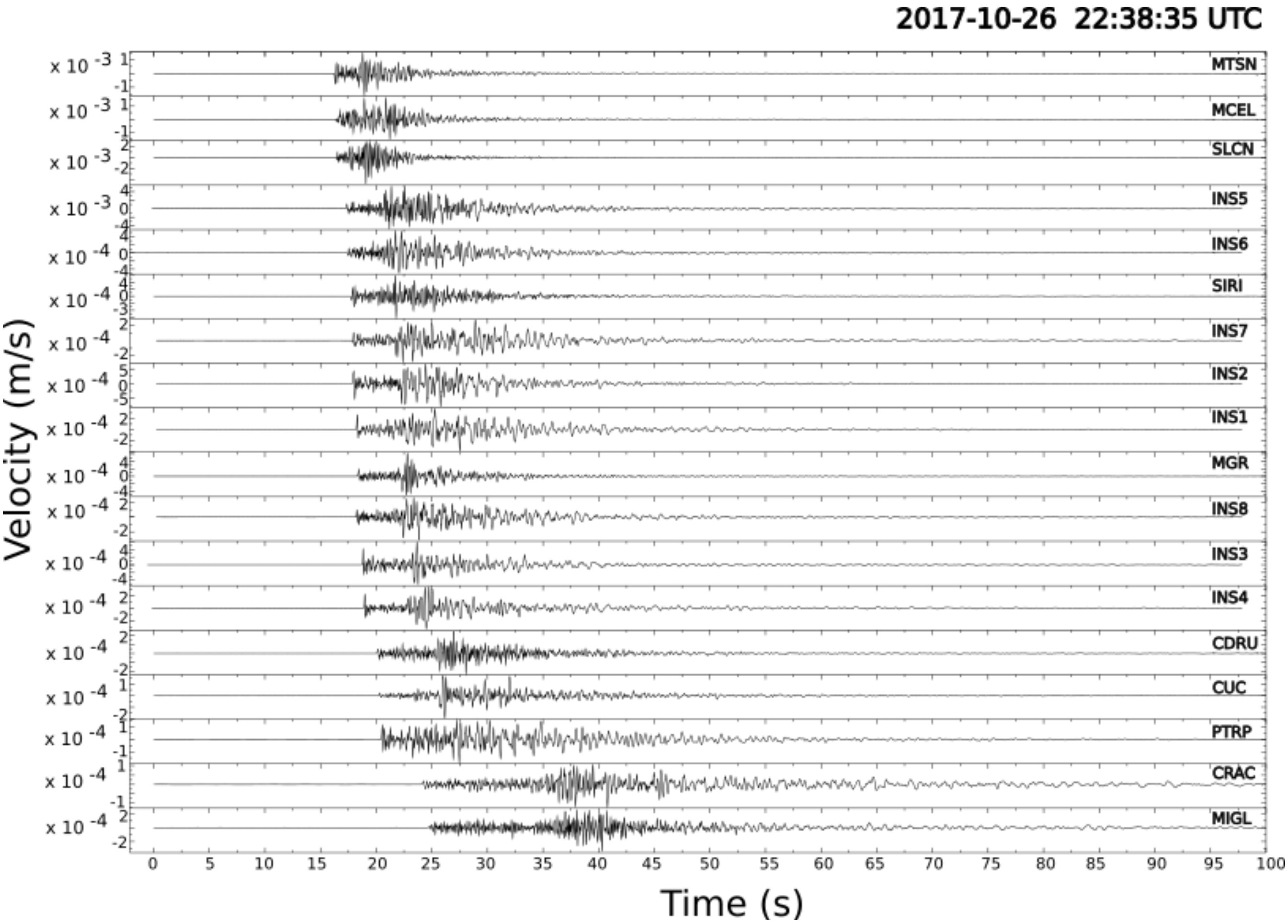

Figure 10: Mw=3.8 local earthquake recorded by the vertical components of the stations belonging to the virtual seismic network composed by INSIEME, INGV and ISNet seismic stations. The traces are sorted, from to the top to the bottom, based on the first P-wave arrival time.

https://doi.org/10.5194/essd-2019-113
Preprint. Discussion started: 5 July 2019

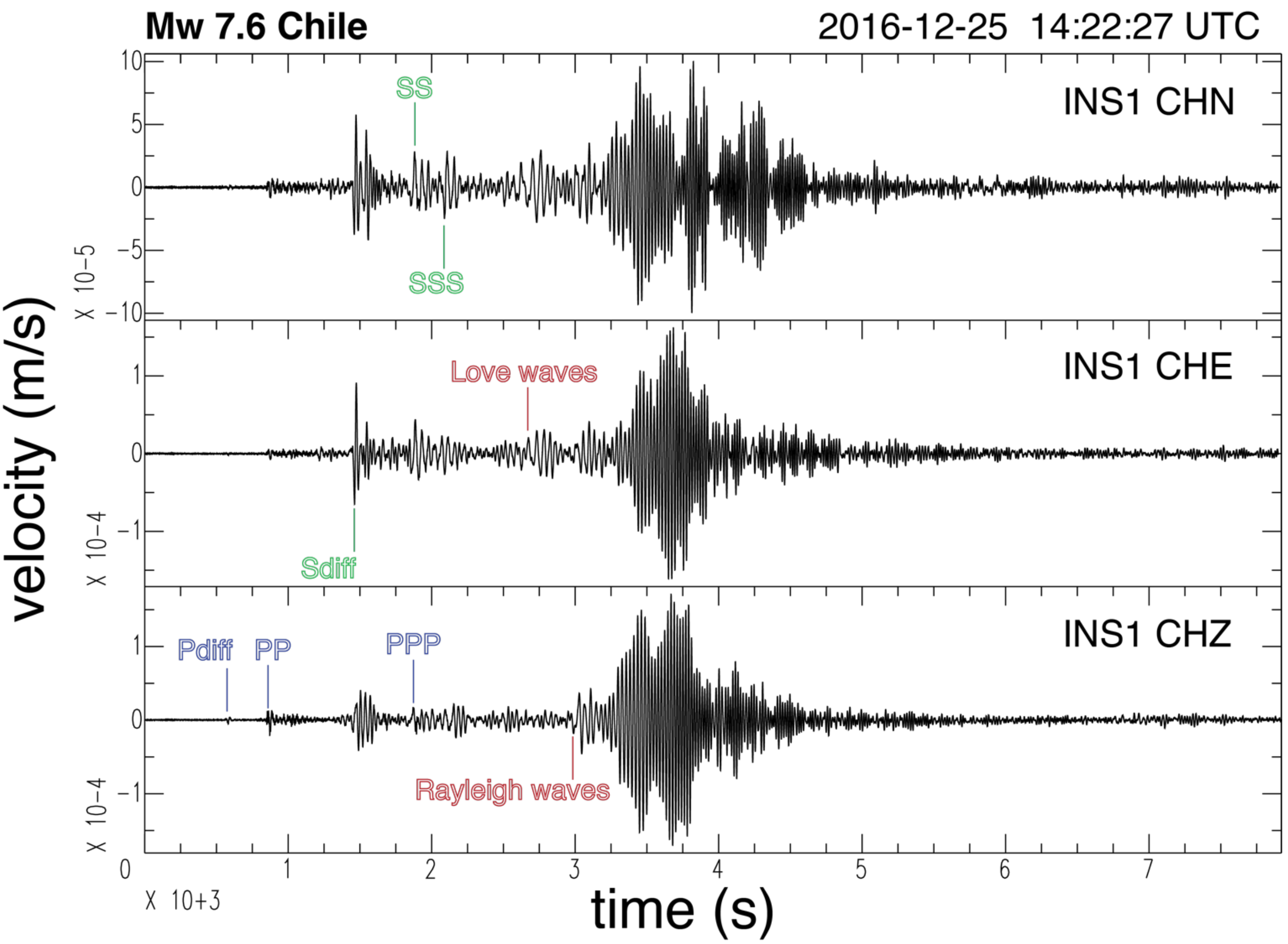

Figure 11: Mw=7.6 Chile earthquake of 2016-12-25 recorded by the three components of the INS1 seismic station. On the top right of the figure the origin time of the teleseism is reported. The theoretical arrival times of the most important recorded seismic phases are shown. The original horizontal components were rotated counter-clockwise by an angle of 307.8° with respect to the North, according to the computations described in detail in section 2.2.